ACS PHYSICAL CHEMISTRY Au
AN OPEN ACCESS JOURNAL OF THE AMERICAN CHEMICAL SOCIETY

pubs.acs.org/physchemau

Perspective

# Probing Anion−Molecule Complexes of Atmospheric Relevance Using Anion Photoelectron Detachment Spectroscopy

Caroline Chick Jarrold*

Cite This: *ACS Phys. Chem Au* 2023, 3, 17−29

Read Online

ACCESS | Metrics & More | Article Recommendations

**ABSTRACT:** Bimolecular reaction and collision complexes that drive atmospheric chemistry and contribute to the absorption of solar radiation are fleeting and therefore inherently challenging to study experimentally. Furthermore, primary anions in the troposphere are short lived because of a complicated web of reactions and complex formation they undergo, making details of their early fate elusive. In this perspective, the experimental approach of photodetaching mass-selected anion−molecule complexes or complex anions, which prepares neutrals in various vibronic states, is surveyed. Specifically, the application of anion photoelectron spectroscopy along with photoelectron−photofragment coincidence spectroscopy toward the study of collision complexes, complex anions in which a partial covalent bond is formed, and radical bimolecular reaction complexes, with relevance in tropospheric chemistry, will be highlighted.

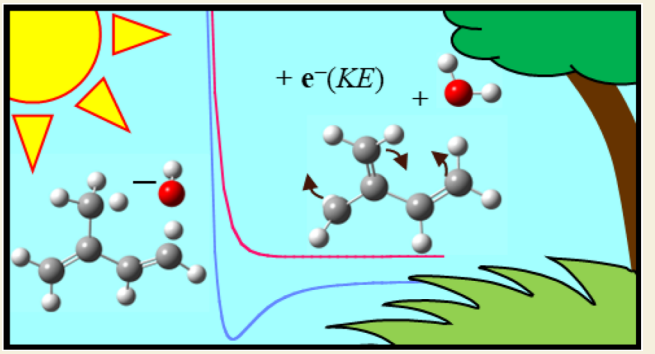


**KEYWORDS:** *ion−molecule complex, collision complex, atmospheric reaction complex, autodetachment, noncovalent-bound states of anions, anion photoelectron spectroscopy*

## 1. INTRODUCTION

Anion photoelectron (PE) spectroscopy has proven to be a powerful tool for studying an astonishingly wide range of chemical species, ranging from single atoms,[1] to bare[2] or ligated[3] nanocrystals, to large biomolecules[4] and beyond.[5] The attributes of the method (ability of $m/z$ selection of the species of interest prior to spectroscopic interrogation, relatively low number densities of the species required, the $\Delta s = \pm 1/2$ selection rule allowing access to different spin states of the neutral, among others) have enabled very meaningful studies of complex systems, far too numerous to list. One particularly appealing feature of this method is that information about both the initial anionic state(s) and the final neutral state(s) can be gleaned from the anion PE spectra.

This perspective will focus on the study of *bimolecular* complexes of atmospheric relevance by photodetachment of anionic species. In this context, the spectroscopic method is, in its simplest form,

$$A^-{\cdot}B \xrightarrow{h\nu} A{\cdot}B + e^-(KE) \quad (1)$$

where $A^-{\cdot}B$ represents the anionic precursor of the bimolecular complex A·B, which is detached with photon energy $h\nu$. The resulting electron kinetic energy ($e^-KE$) is measured to determine the energy of the final state of the neutral complex relative to the anion. Insights from these studies on the fate of primary anions in the troposphere as well as transient neutral collision and reaction complexes will be highlighted. Note that there is a rich history of applying this technique to atmospherically relevant radicals and other reactive species like ozone,[6,7] several examples of which are included in the references.[8−18] This topic would make for an extensive review on its own.

In and of themselves, ion−molecule complexes (IMCs) have historically inspired active scientific exploration because of their importance in gas-phase reactions and photochemistry,[19−27] the properties and dynamics in aqueous electrolytic solutions,[28−30] and physical processes in planetary atmospheres.[31−35] Negatively charged complexes in particular have proven to be fertile ground for study using mass-selective photodetachment spectroscopies, with fundamental physical insights on the anions and their associated neutrals pouring from the laboratories engaged in these studies.[36−52] These species, like cationic IMCs, can accumulate numerous neutral molecules, forming noncovalently bound clusters, a topic explored in a recent review by Sanov.[39]

Received: October 30, 2022
Revised: December 8, 2022
Accepted: December 9, 2022
Published: December 31, 2022





https://doi.org/10.1021/acsphyschemau.2c00060
*ACS Phys. Chem Au* 2023, 3, 17−29

Are anions or anion−molecule complexes relevant in tropospheric chemistry? The broad consensus is that anionic species play a fairly narrow role in the troposphere, mainly contributing to nucleating new particle formation.[53] The number density of anions in the troposphere[54] is on the order of $10^3$−$10^4$ $cm^{-3}$, so 0.1 part per quadrillion (for comparison, the number density of •OH, arguably the most important tropospheric oxidant, ranges from $10^3$ to $10^6$ $cm^{-3}$).[55] Yet, the initial steps leading to new particle formation hold a fundamental allure. Ions are continuously being generated in the air by galactic cosmic rays, radon decay, and $\gamma$ radiation from the soil[56] and from electrification in rainfall and waterfalls.[57,58] Cation formation through any of these mechanisms necessarily involves the production of a free electron, which can then attach to $O_2$, forming $O_2^-$ or, in the case of more energetic electrons, $O^-$ + O. As $O_2$ is the most abundant molecule in the troposphere with a positive electron affinity (EA), $O_2^-$ and $O^-$ are the "primary anions."

As a primary anion, the fate of $O_2^-$ is complex. Figure 1 illustrates a reaction scheme involving both $O_2^-$ and $O^-$ devised

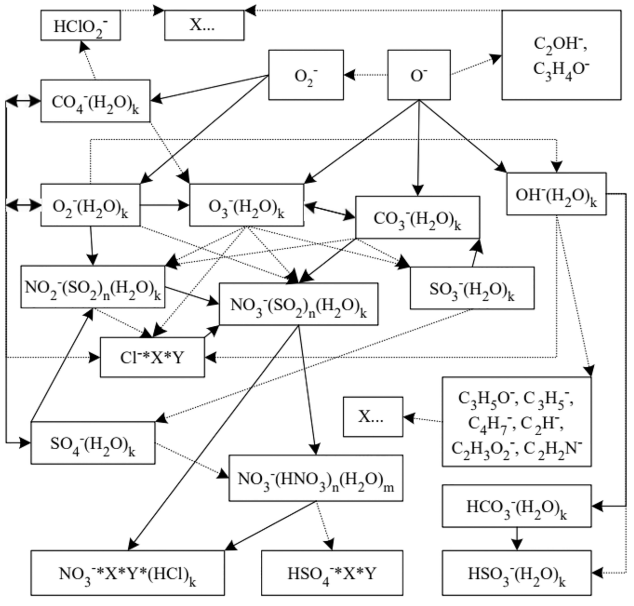


**Figure 1.** Scheme showing the transformation of the primary $O_2^-$ and $O^-$ anions. Reprinted with permission from ref 59. Copyright 2002 Elsevier.

from an early study on the evolution of small air anions.[59] Cluster formation reactions with other atmospheric molecules, charge transfer from $O_2^-$ to species with higher EAs such as •OH, $CO_x$, $NO_x$, or $SO_x$ with subsequent clustering, contribute to the very short lifetime of tropospheric $O_2^-$.[54] Reactions and cluster growth, of course, start with simple IMC formation. However, not all IMCs are alike. For example, $O_2^-$ can couple with a neutral $O_2$ molecule to form a fairly strongly bound anion in which the charge is delocalized over both $O_2$ molecules and would be more appropriately described as $O_4^-$.[60−63] In contrast, if $O_2^-$ couples with an $N_2$ molecule, which has a negative EA, the resulting IMC would be weakly bound and described more appropriately as $O_2^-$·$N_2$. Of course, $N_2O_2$ can take other forms of complex anions,[64] underscoring the complex nature of atmospheric chemistry.

Charge sharing within an anionic complex formed by the association of an anion and a neutral of the same molecule (e.g., above, $O_2^-$ + $O_2$) is not surprising since both molecules have identical EA. This effect has also been evident in larger molecular systems such as biacetyl[65] and benzoquinone.[66] Larger unary complexes have the additional interesting feature of modeling the solvated electron.[67−69] The situation is more complex in heterobimolecular complexes in which both species have positive but unequal EAs. Whether and how charge is shared depends not only on the relative EAs but also on other physical attributes of the molecules, such as polarizability, dipole moment, presence of electrophilic centers, and ability to form hydrogen bonds.

Beyond probing the nature of anionic complexes that lie along the path connecting primary anions and larger complexes and particles, negatively charged IMCs provide a back door for studying neutral collision complexes and reaction complexes. For example, photodetachment of an $HO^-$·X ion molecule complex can prepare a neutral OH radical in reactive distance from the X molecule.

In the following sections of this perspective, the application of anion photodetachment spectroscopies applied toward anion−molecule complexes with relevance in atmospheric chemistry will be surveyed. First, the photodetachment of ion−molecule complexes in which the definitive charge carrier is $O_2^-$ will be explored: These $O_2^-$·X complexes offer a backdoor view of fleeting neutral collision complexes as well as information on how strongly this primary anion interacts with other molecules (X) present in the troposphere. For cases in which charge delocalization across both molecular species occurs, anion PE spectra of the complex anion shows how tightly bound the excess electron becomes. Finally, an overview of the use of complex anions as precursors to radical reaction complexes will be offered.

## 2. INTERMOLECULAR BINDING IN ANION−MOLECULE COMPLEXES AND INSIGHTS INTO NEUTRAL COLLISION COMPLEXES, STUDIED BY ANION PHOTODETACHMENT

As noted above, anion photodetachment techniques provide spectroscopic information on both the initial anion and the final neutral states. As a primary ion, $O_2^-$ can interact with and form complexes with other molecules, and how strongly the $O_2^-$ and partner molecule interact is reflected in the anion PE spectrum. The effect of neutral $O_2$−X repulsion is also reflected in the spectrum, as will be described below.

To set the stage for the following discussion, Figure 2 shows Leonard−Jones potentials generated using typical neutral van der Waals binding energies (ca. 0.05 eV) and intermolecular distances for the three low-lying neutral states of neutral $O_2$ with a hypothetical atmospherically relevant molecular partner (X) along with the potential for the more strongly interacting but noncovalent $O_2^-$·X ion−molecule complex. From the figure, the energy required to detach the electron from the IMC is clearly greater than that for the isolated $O_2^-$ molecular ion. This effect is referred to as a solvent shift or microsolvation of the ion. Put another way, the EA of the $O_2$·X van der Waals complex is higher than that of isolated $O_2$ by an amount *approximately* equal to the solvation energy or the energy required to dissociate X from $O_2^-$.

The PE spectrum is the distribution of kinetic energies of electrons ($e^-KE$) detached from anions via eq 1, where $e^-KE$ is


https://doi.org/10.1021/acsphyschemau.2c00060
ACS Phys. Chem Au 2023, 3, 17−29

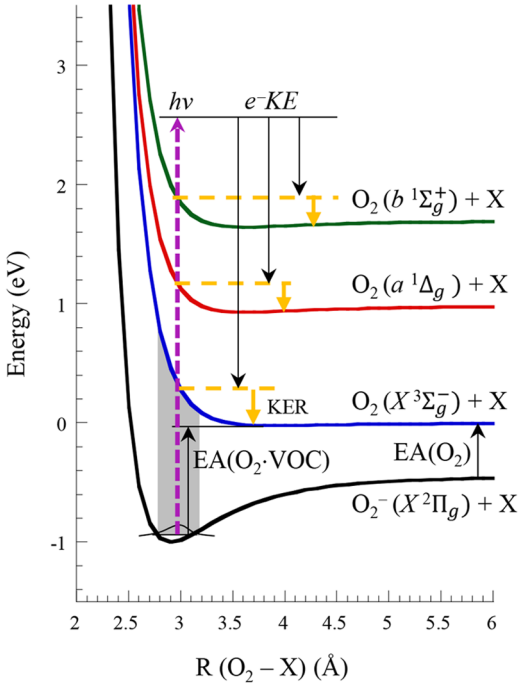


**Figure 2.** Leonard–Jones potentials for a general, innocent $O_2^-$·X ion–molecule complex (black trace) and three low-lying neutral states of the associated van der Waals complexes (blue, red, and green traces) accessible by detachment of the anion using 3.5 eV photon energy (purple, dashed arrow). Representative electron kinetic energies ($e^-KE$, black arrows) resulting from the vertical detachment process in which the neutral bimolecular complex will undergo kinetic energy release (KER, orange arrows) associated with the repulsive potential. EAs of both the van der Waals complex and the bare $O_2$ are included. Adapted with permission from ref 83. Copyright 2016 American Chemical Society.

related to the photon energy ($h\nu$), the neutral EA, and the internal energy of the final neutral state (electronic, rotational, vibrational: $E_{int}^{neutral}$) and that of the initial state of the anion ($E_{int}^{anion}$)

$$e^-KE = h\nu - EA - E_{int}^{neutral} + E_{int}^{anion} = h\nu - e^-BE \quad (2)$$

The electron binding energy ($e^-BE$) is the photon energy-*independent* difference in energy between the final neutral and the initial anion states. Figure 2 includes arrows representing the energy of the detachment photon $h\nu$ and representative $e^-KE$ values. The associated $e^-BE$ values are simply $h\nu - e^-KE$, and PE spectral features measured using different photon energies should appear at constant $e^-BE$. Exceptions to this rule include indirect processes, such as

$$A^-\cdot B \xrightarrow{h\nu} A\cdot B^- \xrightarrow{\tau} A + B + e^-(KE) \quad (3)$$

Photoexcitation to an excited state of the anionic complex, such as the charge-transfer state suggested by eq 3, can yield electrons with kinetic energies independent of the photon energy. Examples of this spectroscopic signature will be presented in section 3.

Descriptions of how ions are produced and the various ways photoelectron spectral measurements are made can be found in numerous publications, several of which are included here.[6,7,15,36,47,48,60,63,70]

An example of how charge localization on $O_2^-$ is reflected in the PE spectrum of an $O_2^-$·X complex is shown in Figure 3, with

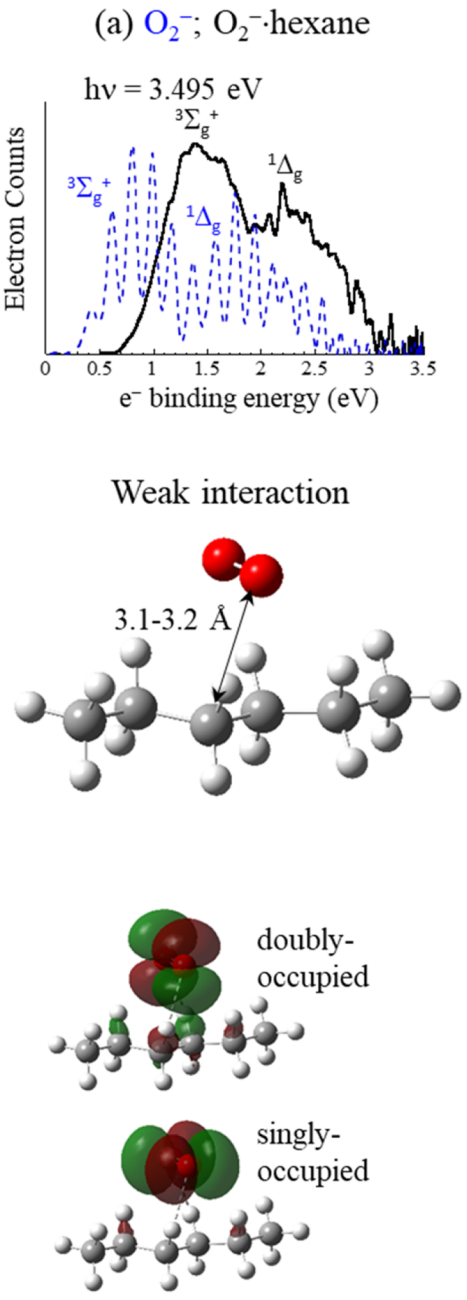


**Figure 3.** Representative PE spectrum of $O_2^-$·hexane (hexane = innocent neutral partner in the ion–molecule complex) compared to bare $O_2^-$, along with the computed (CAM-B3LYP/aug-cc-pVTZ) structure and frontier orbitals of the anion. Adapted with permission from ref 96. Copyright 2021 American Chemical Society. PE spectrum of $O_2^-$·hexane adapted with permission from ref 83. Copyright 2016 American Chemical Society.

the assumption that X is an "innocent" partner in this complex (charge distinctly localized on $O_2^-$, and X does not undergo significant molecular or electronic structural changes in the process of complex formation). The top panel shows the PE spectrum of both isolated $O_2^-$ (blue dotted trace, calibrated using a previously published spectrum[71]) and $O_2^-$·hexane (black solid trace). The $O_2^-$ PE spectrum shows series of peaks spaced by the vibrational frequency of $O_2$, or a vibrational progression, in both the ground $^3\Sigma_g^-$ state and the low-lying $^1\Delta_g$ state (an


https://doi.org/10.1021/acsphyschemau.2c00060
ACS Phys. Chem Au 2023, 3, 17–29

additional progression associated with the low-lying $^1\Sigma_g^+$ state overlaps with the high-$e^-BE$ portion of the $^1\Delta_g$ vibrational progression). The spectrum of $O_2^-$·hexane is shifted to higher $e^-BE$, as expected from Figure 2. In addition, the transitions to individual vibrational levels of $O_2$ are not resolved: As shown in Figure 2, along the $O_2$–hexane intermolecular coordinate, the minimum energy structure of the anion corresponds to a repulsive part of the neutral potential, so previously resolved vibrational features are convoluted with continuum signal. Indeed, we would anticipate the neutral molecules to have a kinetic energy of ca. 0.05 eV upon detachment.

The molecular structure of $O_2^-$·hexane is shown below the spectrum along with the frontier orbitals of the anionic complex, which closely resemble the $\pi_g$ orbitals of $O_2^-$. Importantly, what the data and calculations suggest is that the primary anion, $O_2^-$, interacts noncovalently with a nonpolar but polarizable hydrocarbon. The energy required to dissociate the anion–molecule complex is 0.48 ± 0.05 eV based on the solvent shift, which is far greater than the average collision energy at room temperature (ca. 0.06 eV).

More strongly bound complexes such as the venerated $O_2^-$·$H_2O$ complex[72−76] can still be largely characterized as innocent. Numerous studies have shown that the charge does indeed remain localized on the $O_2$ portion of this particular complex. The PE spectra obtained by Continetti and co-workers,[76] which is shown in Figure 4 (also obtained by Johnson and co-workers[72] and Sanov and co-workers[74,75]), show a large ca. 1 eV solvent shift. The additional information gleaned in measurements made by Continetti and co-workers is the narrow 0.12 eV kinetic energy release by the neutral molecular partners upon photodetachment, which reflects the repulsion between the two neutrals.[76] Circling back to the fate of $O_2^-$ in the troposphere, it is clear that the thermodynamic driving force for noncovalently bound complex formation is nontrivial.

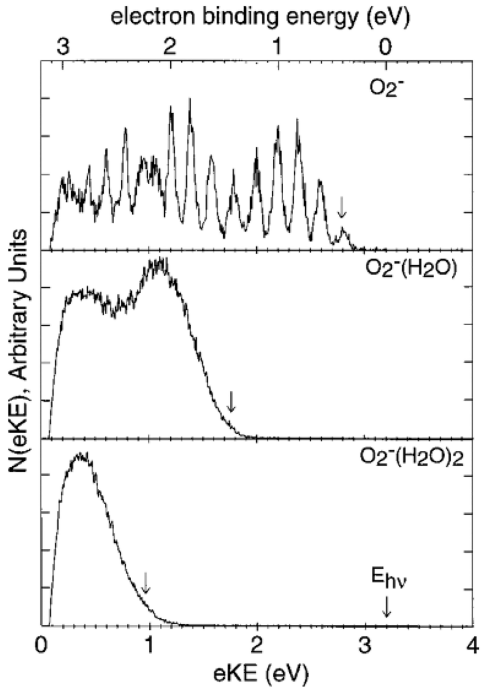


**Figure 4.** PE spectra of $O_2^-$, $O_2$·$H_2O$, and $O_2(H_2O)_2^-$ measured using 3.2 eV photon energy, reported by Continetti and co-workers. These results show the large shift in binding energy of the $O_2$·$H_2O$ complex relative to bare $O_2$ along with the broadening of spectral features. $O_2^-$·$H_2O$ represents a strongly interacting anion–neutral pair, as reflected in the large "solvent" shift, but with the excess charge localized on the $O_2^-$. Reproduced with permission from ref 76. Copyright 2001 AIP Publishing.

The heading of this section also refers to neutral collision complexes. In their simplest form, atmospheric collision complexes are bimolecular systems that, for their ca. picosecond lifetimes, have symmetries and, to a lesser extent, molecular structures that differ from the individual separated molecules. With the lower symmetry of the collision complex, electronic and vibrational transitions that are forbidden in the isolated molecules may become allowed in the collision complex. This effect has been known since the early 20th century.[77] More recent studies have considered the contribution of collision complexes such as $O_2$–$O_2$, $O_2$–$N_2$, and $N_2$–$H_2O$ to the solar energy budget.[78−81] The atmosphere-abundant homonuclear diatomic molecules, $N_2$ and $O_2$, have no allowed electronic, vibrational, or rotational transitions that would contribute to the greenhouse effect, but while undergoing collisions, they can contribute appreciably.[82]

Our previous studies on $O_2^-$·X ion–molecule complexes suggest that the energy of the $^1\Delta_g$ state of the neutral $O_2$ undergoing a collision changes with the identity of X.[83,84] Figure 5 shows the PE spectra and spectral fits of bare $O_2^-$ (Figure 5a) and a series of $O_2^-$·X complexes (Figure 5b–f). The fits facilitate a more systematic determination of the change in EA with X along with the change in the term energy of the singlet state.

From the spectral fits, the following was learned. For nonpolar X molecules [X = hexane (Figure 5b) and isoprene (Figure 5c)], the $a^1\Delta_g - X^3\Sigma_g^-$ splitting remained within 0.05 eV of that of bare $O_2$ [$T_0$ ($a^1\Delta_g$) = 0.977 eV]. However, in the case of X = acetone (Figure 5d), which has a large dipole, $T_0$ ($a^1\Delta_g$) = 0.83 eV. For polar partners capable of hydrogen bonding [X = EtOH (Figure 5e) and 3-buten-2-ol (Figure 5f)], $T_0$ ($a^1\Delta_g$) is below 0.8 eV. Why is there an apparent change in the term energy of the singlet state? Both the anion and the singlet neutral state have electrons paired in the now nondegenerate $\pi^*$ orbital pointing toward X, suggesting that this component is more stabilized by the presence of X than the $\pi^*$ that can be described as more parallel to X (see the singly and doubly occupied orbitals depicted in Figure 3). While the singlet state of the neutral van der Waals complex is still higher in energy than the triplet state, it is more stabilized relative to the $^1\Delta_g$ state of bare $O_2$ than the triplet state is relative to the $^3\Sigma_g^-$ state because of the relative stability of the $\pi^*$ orbital pointing towards X.

There are limitations to this approach to studying transient collision complexes. The measurements described above are low resolution, though we note here that collision-induced absorption lines are also broad, ca. 400 $cm^{-1}$.[85] In addition, the spectroscopic information is averaged over a distribution of repulsion (collision) energies predetermined by the specific attributes of X, rather than the ambient temperature of the neutral gas. In the case of X = polar, the structure of $O_2^-$·X is well defined, so the neutral structure being probed is strongly biased toward a specific collisional orientation, not averaged over a range of relative molecular orientations or impact parameters.

Nonetheless, information gleaned from these studies represents a small piece of a larger puzzle: The identity of the collision partner of $O_2$ affects the spectral range of collision-induced absorption, if modestly. The $O_2^-$–X (noncovalent) binding energy has been determined for a number of X partners. These data could eventually inform models of atmospheric


https://doi.org/10.1021/acsphyschemau.2c00060
ACS Phys. Chem Au 2023, 3, 17−29

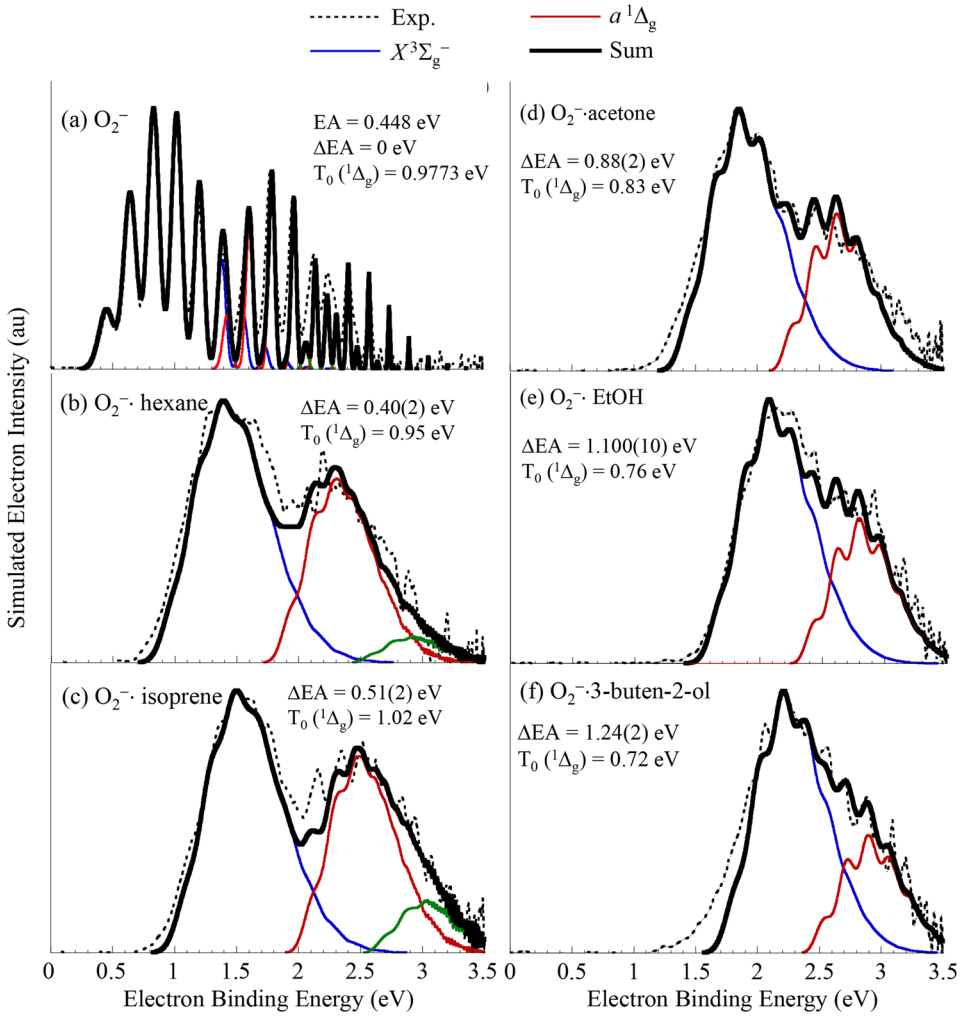


**Figure 5.** PE spectra of (a) $O_2^-$ and (b–f) $O_2^-$·X (dashed lines) along with spectral simulations (solid black) used to determine the relative energies of the neutral states correlating with the $^1\Delta_g$ (blue), $^1\Sigma_g^+$ (green), and $^3\Sigma_g^-$ (red) neutral final states of $O_2$ in the van der Waals complexes. Left column, X = the nonpolar (b) hexane and (c) isoprene molecules. Right column, X = (d) polar acetone molecule, (e) polar and H-bond-forming ethanol molecule, and (f) polar, polarizable, and H-bond-forming butenol molecule. ΔEA values are the shift in the origins of the simulated spectra of the complexes relative to the bare $O_2^-$ simulation, and $T_0$ ($^1\Delta_g$) represents the simulated origin of the first excited state relative to the simulated origin of the $^3\Sigma_g^-$ state. Note that this value is lower for polar partners. (a–c) Adapted with permission from ref 83. Copyright 2016 American Chemical Society. (d–f) Adapted with permission from ref 84. Copyright 2017 American Chemical Society.

reaction pathways involving the primary $O_2^-$ anion as well as models of the greenhouse effect.

We note here that there is a substantial body of complementary work probing direct absorption, photosensitization, and production of singlet oxygen from photoexcitation of neutral $O_2$·X van der Waals or encounter complexes,[85−93] which could easily be the topic of its own perspective.

## 3. $[O_2–M]^-$ COMPLEX ANIONS

Complexes formed between $O_2^-$ and other molecules in the troposphere can be simple ion−molecule complexes as described in the previous section, a complex anion in which charge is shared, or, in other words, a partial covalent bond is established. The $O_4^-$ noted above is an example. The situation is more complicated for heteromolecular species with different, but both positive, EAs as well as differences in other properties such as polarizability, dipole moment, hydrogen-bond donor availability, etc. Figure 6 shows a hypothetical scenario in which two molecules, A and B, form an anion−molecule complex. In this scenario, molecule A has a lower EA than molecule B but A has low polarizability. In contrast, B is highly polarizable, polar, or perhaps a H-bond donor (or any combination thereof). At infinite A + B separation, A + $B^-$ is clearly more stable than $A^-$ + B because the EA of B is higher. However, as A and $B^-$ come into proximity, the resulting $B^-$·A ion−molecule complex is less stable than $A^-$·B, since the polar or H-bond-donating B molecule stabilizes $A^-$ more than the nonpolar neutral A molecule stabilizes $B^-$.

Further, the fact that both A and B can bind an electron gives rise to the possibility that the excess charge will be delocalized between A and B with concomitant partial covalent bond formation.[94] In this case, the resulting anion would not be appropriately described as an ion−molecule complex. Rather, it is a complex anion: $[A–B]^-$. Photodetachment of the complex ion breaks this partial bond and results in a neutral van der Waals complex at a strongly repulsive intermolecular distance. This effect is represented in Figure 6: The energy of the neutral complex in the structure of the $[A–B]^-$ complex anion lies significantly above the A + B dissociation limit. The difference


https://doi.org/10.1021/acsphyschemau.2c00060
ACS Phys. Chem Au 2023, 3, 17−29

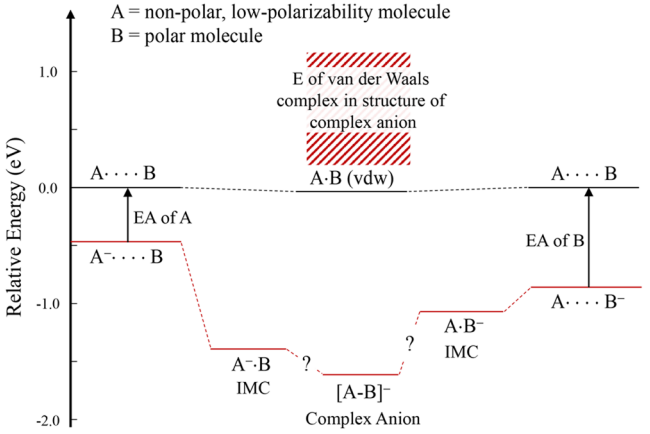


**Figure 6.** Schematic of energies of different hypothetical anion−molecule complexes in which molecules A and B both have positive but different electron affinities as well as physical attributes. IMC stands for ion−molecule complex, which assumes charge is distinctly localized on one of the two molecules in the bimolecular complex anion. $[A{-}B]^-$ suggests charge delocalization and partial covalent bond formation between the two constituents. Relatively flat energy landscape of the neutral A·B van der Waals complex along with the molecules at infinite separation is also included for reference. Because of the partial bond in the $[A{-}B]^-$ complex, photodetachment of the electron prepares a neutral complex that is distorted and therefore higher in energy than the optimized structure of the A·B van der Waals complex.

between this energy landscape and that depicted in Figure 2 is that in the case of the $[A{-}B]^-$ complex anion, the spatial extent of the wave function along the A—B intermolecular coordinate for the anion overlaps with a much more highly repulsive part of the neutral intermolecular potential. In addition, there are two bound anionic asymptotes. Photodetachment experiments that measure electron kinetic energy in coincidence with the kinetic energy release of the neutral molecules, such as those developed by Continetti, provide a direct measure of the repulsion between the two neutral molecules prepared by detachment of the anion.[61−63,95]

Taken a step further, there can be instances of partial covalent bond formation between an anion and a neutral that has a negative EA (cannot bind an electron as an isolated molecule) but with a corresponding noncovalently interacting neutral van der Waals complex. Both cases will be touched on here, in the context of the $O_2^-$ primary anion, with its modest EA of 0.448 eV (e.g., molecule "A" in Figure 6).[71]

The first case described above, in which both molecules in a heterobimolecular complex have positive electron affinities, can be more deeply explored by systematically varying the properties of one of the partner molecules via functionalization. A recent example[96] of this approach is the study of $O_2^-{\cdot}M$, where $M$ = glyoxal (or ethanedial, OCHCHO; EA = 1.10 ± 0.02 eV),[97] methyl glyoxal (EA = 0.87 ± 0.02 eV),[98] and dimethyl glyoxal (EA = 0.69 ± 0.02 eV).[65] The singly occupied molecular orbitals in $M^-$ can be described as a $\pi$ bond that is antibonding with respect to the two C═O bonds and bonding with respect to the central C−C bond. Substitution an −H atom for a $-CH_3$ group destabilizes this orbital, resulting in the decrease in EA with methyl substitution.

Glyoxal and its methylated analogs have relevance in tropospheric chemistry. Glyoxal is used to trace reaction pathways of biogenic compounds in the troposphere,[99,100] and it contributes to secondary organic aerosol formation.[101,102] The molecule with its close-lying $C_{2v}$ and $C_{2h}$ (historically referred to as cis and trans) isomers and its low-lying triplet states has made for interesting spectroscopic and theoretical investigations.[103−111] Methylglyoxal is the product of oxidation of several volatile organic compounds in the troposphere,[112−117] while dimethylglyoxal, or biacetyl, is produced by ring cleavage from $NO_x$ oxidation of aromatics.[118−120] These molecules have also been actively investigated spectroscopically.[121−128]

Figure 7 shows how different the anion PE spectra of the complex anions formed between $O_2$ and $M$ = glyoxal (Figure

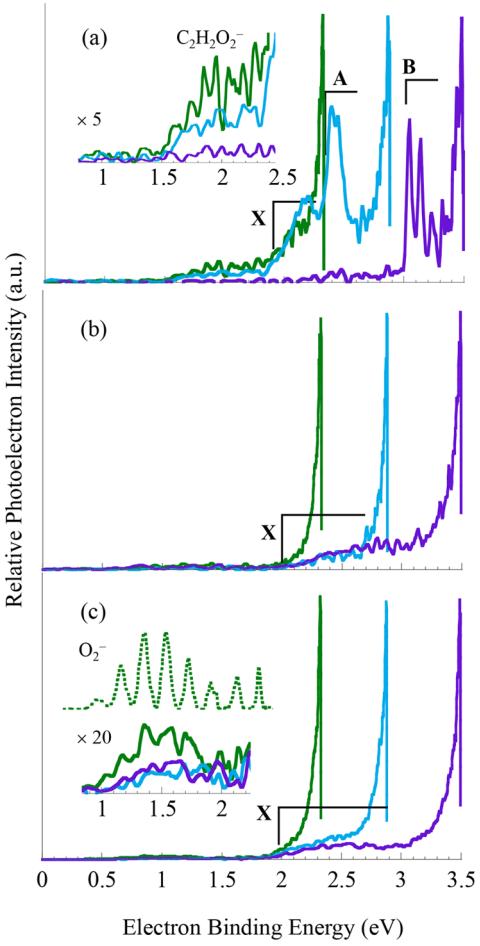


**Figure 7.** Anion PE spectra of (a) $[O_2$-glyoxal$]^-$, (b) $[O_2$-methylglyoxal$]^-$, and (c) $[O_2$-biacetyl$]^-$ complexes obtained using photon energies of 2.330 (green), 2.883 (blue), and 3.495 eV (purple). Features labeled X are attributed to direct detachment transitions, while intense signal at the high $e^-BE$ edge of each spectrum is attributed to an indirect electron ejection process. (Insets) Signals attributed to two-photon processes in which the first photon dissociates the complex anion and the second photon detaches the daughter anion. Adapted with permission from ref 96. Copyright 2021 American Chemical Society.

7a), methylglyoxal (Figure 7b), and biacetyl (Figure 7c) are from the typical solvent-shifted and broadened PE spectrum of $O_2^-$ seen for innocent $O_2^-{\cdot}X$ ion−molecule complexes (e.g., Figure 6b). In particular, they are dominated by electrons with near-zero kinetic energy regardless of photon energy! This spectroscopic feature is the signature of an indirect detachment process noted above, such as thermionic emission of the electron from a short-lived excited anion state such as a highly


https://doi.org/10.1021/acsphyschemau.2c00060
ACS Phys. Chem Au 2023, 3, 17−29

vibrationally excited ground state of the anion, a quasibound excited electronic state, or a charge-transfer state (e.g., eq 3). Alternatively, autodetachment from quasibound vibrational levels of a nonvalence-bound state, such as a dipole-bound or correlation-bound state, of the anion can also lead to distinct $e^-KE$s that are independent of the photon energy.[129,130]

Indirect detachment might be expected if the Franck−Condon overlap between the anion and the neutral lies "behind" the repulsive wall (i.e., the energy of the neutral van der Waals complex in the structure of the anion is higher than the photon energy used to detach the anion), making the cross section for direct detachment to the neutral vanishingly small. In this case, direct detachment signal, labeled **X** in Figure 7, was observed. There is also evidence of photodissociation and detachment of daughter ions in the spectra, with the glyoxal anion carrying the charge in photodissociation of $[O_2{-}\text{glyoxal}]^-$ and $O_2^-$ carrying the charge in photodissociation of $[O_2{-}\text{biacetyl}]^-$, suggesting that EA plays some role in which photodissociation channels are favored.

Aside from the photodissociation, the fact that both indirect and direct detachment processes are observed suggests that there is nonzero Franck−Condon overlap with the neutral but that the absorption cross section to an anion excited state common to all three complexes was larger. For reasons detailed in the original publication, a dipole-bound state supported by the *cis-M* conformers appears to be the most likely explanation.

How is the electronic structure of the $[O_2{-}M]^-$ complex described? The excess charge is indeed delocalized between $O_2$ and *M*, so a partial covalent bond is formed between the two constituents, but $O_2$ carries more charge than *M*, despite *M* having a higher EA than $O_2$ in this case. Figure 8 shows the LUMO, HOMO, and SOMO of the $[O_2{-}\text{glyoxal}]^-$ complex anion along with the $\pi_3$ orbital of glyoxal, which is the SOMO of the glyoxal anion, and a $\pi_g$ orbital of $O_2$. The HOMO of $[O_2{-}\text{glyoxal}]^-$, which is the orbital associated with detachment to the lowest energy neutral limit, $O_2\,^3\Sigma_g^- + \text{glyoxal}\ ^1A_1$, is delocalized across both molecules but has more amplitude attributable to the $\pi^*$ orbital on $O_2$ (correlated with the $\pi_g$ orbital of isolated $O_2$), and the LUMO has more glyoxal-local $\pi_3$ character. There are several low-lying excited states of this anion that lie below the detachment continuum, including what would nominally be described as a charge-transfer state (LUMO ← HOMO transition), potentially giving rise to a rich, IR *electronic* absorption spectrum for these and related complex anions.

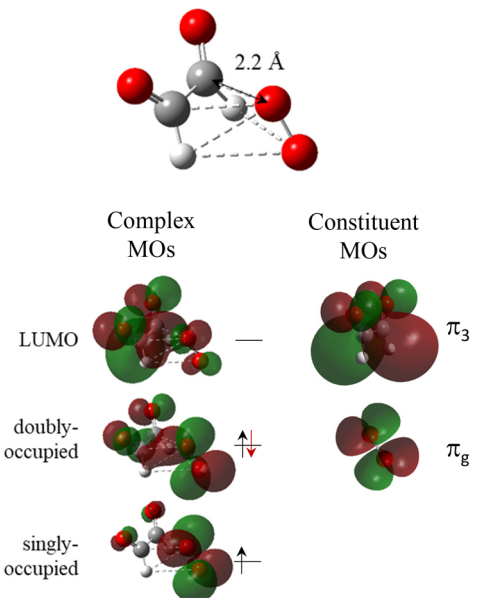


**Figure 8.** Anion molecular structure and frontier orbitals of the $[O_2{-}\text{glyoxal}]^-$ complex anion, highlighting the small O−C internuclear distance (ca. 2.2 Å relative to the O−C internuclear distance in the $O_2^-$·hexane ion−molecule complex (ca. 3.2 Å, Figure 3) between the two species, as well as the $O_2$ and glyoxal orbital mixing, based on CAM-B3LYP/aug-cc-pVTZ calculations on both anions. Adapted with permission from ref 96. Copyright 2021 American Chemical Society.

Partial covalently bound complex anions also form between $O_2^-$ and species with negative EA. One of the products of tropospheric $O_2^-$ reactions included in Figure 1 is $CO_4^-(H_2O)_k$, implicating $O_2^-$ association with $CO_2$. Isolated $CO_2$ has a negative electron affinity, though as detailed by Weber in an insightful review,[131] $CO_2$ can interact quite strongly with anions because of the electrophilicity of the C atom. Charge−quadrupole interactions and charge transfer can lead to significant O−C−O nonlinearity, which layers in charge−dipole interactions. In the specific case of $O_2^- + CO_2$, a partial covalent bond is formed between the two molecules,[132,133] creating an anion with high vertical detachment energy, as shown by Kim and co-workers.[134] This is a noteworthy case in which the adiabatic electron detachment energy of $CO_4^-$ (i.e., the adiabatic electron affinity of the $O_2{\cdot}CO_2$ van der Waals complex) is modest, ca. 1.5 eV, but the cross section for detaching to the equilibrium structure of the neutral complex is zero, leading to a particularly high VDE of 4.56 eV.[134]

The thread that connects $CO_4^-$ and $[O_2{-}\text{glyoxal}]^-$ is the electrophilic carbon center of the carbonyl group. From a standard chemistry textbook point of view, the similar orbital energies and good overlap between $O_2/O_2^-$ and C═O frontier orbitals facilitate partial bond formation.

The fate of $CO_4^-$ formation has already been studied (see Figure 1), but what are the potential implications of complex anion formation such as $[O_2{-}\text{glyoxal}]^-$? No studies directly measuring the fate of this complex anion have been published to our knowledge. However, as with all atmospheric ions, anions, or cations, the complex anion could cluster with additional molecules, e.g., $[O_2{-}\text{glyoxal}]^-{\cdot}(H_2O)_n$. This species is a radical (doublet ground state) with a high electron binding energy, so it could potentially be reactive with molecules to which it clusters. Further studies of this and a related complex anion may yield interesting new insights into tropospheric chemical processes.

## 4. NEUTRAL ATMOSPHERIC REACTION COMPLEXES STUDIED BY DETACHMENT OF ANIONIC COMPLEXES

Radicals such as OH, $HO_2$, RO, $RO_2$, etc., generally have positive electron affinities, with the associated anions having relatively stable singlet ground states. These ions play a role in the fate of the primary $O_2^-$ and $O^-$ ions, as illustrated in Figure 1. However, this section gives an overview of how the anions can be used as precursors to *neutral* radical reaction complexes.

An important oxidant in the troposphere is the hydroxyl radical, which can abstract hydrogens from volatile organic compounds, creating radical species that can then form peroxo species from $O_2$ addition, or it can form adducts with unsaturated molecules such as isoprene. In particular, the highly investigated OH−isoprene adduct is itself a radical that can undergo a sequence of reactions that ultimately leads to tropospheric ozone production. Yet, short-lived radical reaction


https://doi.org/10.1021/acsphyschemau.2c00060
ACS Phys. Chem Au 2023, 3, 17−29

complexes are a difficult target for study because they are inherently transient.

Continetti and co-workers demonstrated in several publications how atmospherically relevant radical neutral reaction complexes could be prepared by detaching stable, closed-shell anion−molecule complexes. For example, the group explored the entrance channel of the OH + $CH_4$ → $H_2O$ + $CH_3$ reaction via photoelectron−photofragment coincidence spectroscopy of the $OH^-{\cdot}CH_4$ ion molecule complex.[135] Their study established that $CH_4$, when in the $OH^-{\cdot}CH_4$ complex, is slightly distorted relative to isolated $CH_4$, since vibrational excitation of $CH_4$ was evident in the photoelectron spectrum. A similar study was conducted on the $OH^-{\cdot}C_2H_4$ ion−molecule complex.[136] Their results provided insight into the dynamics of the entrance channel of the abstraction reaction.

Showing the versatility of this general strategy for studying reaction dynamics, Continetti and co-workers probed the methoxide−water [$CH_3O^-{\cdot}(H_2O)$] ion−molecule complex as a precursor to the *exit* channel of the $CH_3OH$ + OH → $CH_3O$ + $H_2O$ reaction.[137] The methoxide anion and neutral have been studied extensively using anion photodetachment methods;[138,139] The PE spectrum of $CH_3O^-$ has short, well-resolved vibrational progressions, though affected by vibronic coupling, with an origin at 1.57 eV.[139] The $e^-KE$ distribution resulting from detachment of $CH_3O^-{\cdot}H_2O$, shown in Figure 9 taken from

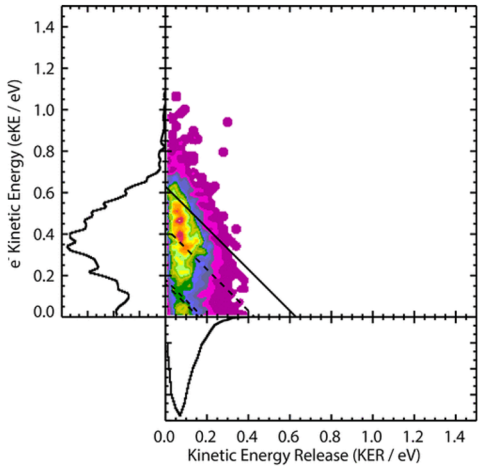


**Figure 9.** Photoelectron−photofragment coincidence spectrum of the $CH_3O^-{\cdot}H_2O$ ion−molecule complex measured using 3.20 eV photon energy. This experiment probes the exit channel of the $CH_3OH$ + OH → $CH_3O$ + $H_2O$ reaction. Diagonal solid line and dashed lines represent the limit to the ground and vibrationally excited neutral product channels. See text for additional details. Reprinted with permission from ref 137. Copyright 2022 American Chemical Society.

ref 137, shows a ∼1 eV solvent shift. However, the broadness of the electron detachment signal coupled with the narrow kinetic energy release of the neutral $CH_3O$ and $H_2O$ daughters along with supporting calculations suggested a relatively long-lived neutral complex with both bend and stretch excitation of the $H_2O$ "product" molecule, again providing insight into the dynamics of this reaction.

The Jarrold group recently reported a similar study of the $OH^-$·isoprene ion−molecule complex,[140] though without the capability of determining the kinetic energy release of the final neutral molecules of the experiments done by Continetti and co-workers. However, using a tunable detachment laser, they demonstrated that −H abstraction by the neutral OH radical could be driven by photodetachment of the $OH^-$·isoprene ion−molecule complex near threshold.

Using photon energies well above the threshold photodetachment of the $OH^-$·isoprene ion−molecule complex, the usual signature of an innocent complex was observed, as shown in Figure 10. That is, compared to the PE spectrum of $OH^-$ (black trace), the spectrum of the $OH^-$·isoprene complex (purple and blue traces) appears shifted to higher $e^-BE$ and is broadened. However, tuning the detachment laser so that energetically the detachment transition produces electrons with near-zero kinetic energy, i.e., at the threshold for detachment, the spectrum exhibits photon-energy-independent features at low $e^-KE$, which, as noted previously, is the signature of an indirect process. Supporting calculations suggested that the OH prepared by photodetachment abstracts an H atom from the methyl group on isoprene. Slow electrons generated with the lowest photon energies get temporarily bound by the large dipole moment created by the nascent H−OH bond. The newly formed isoprenyl radical is simultaneously created in a vibrationally excited state. The overall dipole-bound $H_2O$−[isoprenyl] + $e^-$ then undergoes vibrational autodetachment, with the energy difference between the vibrationally excited dipole-bound state and the resulting neutral state, which is on the order of a vibrational spacing, being carried away by the autodetached electron.

The bottom panel of Figure 10 shows common features (a at $e^-KE$ = 120 $cm^{-1}$; b at $e^-KE$ = 370 $cm^{-1}$; c at $e^-KE$ = 730 $cm^{-1}$) seen in spectra obtained with 2.330 and 2.431 eV with a new feature emerging (asterisk at 530 $cm^{-1}$) with slightly higher photon energy (increasing that the photon energy accesses other vibrational modes of the transient dipole-bound state). These energies are not direct vibrational energy spacings, but they are offset by the modest binding energy of the dipole bound state, which is on the order of tens of $cm^{-1}$. Taking the binding energy into account, these results suggest that the isoprenyl radical is formed with excitation in the backbone twist and distortion modes. Again, this approach to studying radical reaction complexes provides unique insight into the reaction dynamics.

Limitations of this approach lie in the structure of the precursor anion. As an example, the more tropospherically relevant reaction between OH and isoprene involves addition of the OH to one of the carbons along the butadiene backbone.[141−143] The structure of the $OH^-$·isoprene ion−molecule complex, however, is governed by the stability of the nontraditional C−H···$^-$OH hydrogen bond. $OH^-$ is in closest proximity to the methyl H atoms, so the reaction that is initiated by photodetachment is the abstraction reaction. While this reaction is relevant in combustion reactions and a small fraction of reactions in the troposphere, this approach does not provide easy access to the desired adduct formation reaction. However, in a number of cases, such as the $OH^-{\cdot}CH_4$ and $CH_3O^-{\cdot}H_2O$ complexes explored by Continetti and co-workers,[135,137] the structures of the anionic precursors have Franck−Condon overlap with the desired entrance or exit channels of the reactions of interest.

Finally, we note that anionic IMCs of atmospheric relevance have also served as precursors to *anionic* reaction complexes, such as in the case of the $O_2^-{\cdot}H_2O$ complex, revealing details of the $O^-$ + $H_2O$ → $OH^-$ + $^{\bullet}OH$ reaction.[72] New insights on anionic ion−molecule complexes gained in the past decade may inspire additional studies along this line.


https://doi.org/10.1021/acsphyschemau.2c00060
ACS Phys. Chem Au 2023, 3, 17−29

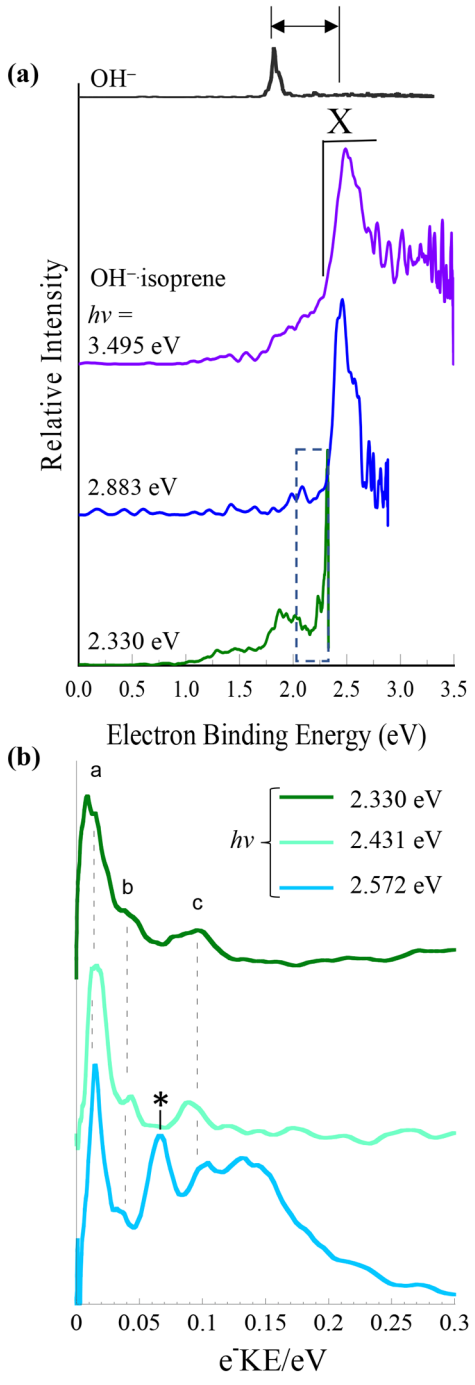


**Figure 10.** (a) Photoelectron spectra of the $OH^-$·isoprene complex measured using three photon energies, compared with the $OH^-$ spectrum measured with 3.495 eV photon energy. PE spectra of $OH^-$·isoprene measured with photon energies above threshold photodetachment (3.495 and 2.883 eV) are typical of a simple ion–molecule complex in which the charge is carried by $OH^-$; 2.330 eV spectrum shows sharp features at the high $e^-BE$ edge (low $e^-KE$ edge). (b) PE spectra of the $OH^-$·isoprene complex plotted in terms of $e^-KE$ (corresponding to the $e^-BE$ range indicated by the dashed box in a), showing that at three photon energies in the threshold detachment range, i.e., producing electrons with near-zero kinetic energy, low $e^-KE$ features appear to be independent of photon energy, suggesting an indirect detachment process. (a and b) Adapted with permission from ref 140. Copyright 2020 American Chemical Society.

## 5. SUMMARY AND OUTLOOK

The chemistry of the troposphere is a complex web of processes that depend on numerous, often coupled factors. The troposphere, which is not an isolated system in chemical parlance, still has unknown sinks and sources of reactants and pollutants. Negative ions have not generally been considered significant participants in atmospheric chemistry, yet $O_2^-$ has recently been implicated as an intermediate in $H_2SO_4$ formation on soot, along with the more recognized OH radical reactant.[144]

This perspective has surveyed the application of one tool, anion photodetachment techniques, toward the study of several types of bimolecular anionic complexes with relevance in tropospheric chemical and physical processes. These studies provide direct insight into the energy of the noncovalent bond formed between the primary $O_2^-$ anion and different neutral partner molecules. These studies also reveal phenomena such as how the spin- and symmetry-forbidden $^1\Delta_g - {}^3\Sigma_g^-$ transition of $O_2$, which becomes allowed while $O_2$ is undergoing a collision, has collision-partner energy dependence.

$O_2^-$ was also shown to form partial covalent bonds with atmospherically relevant molecules having a carbonyl group, such as glyoxal or $CO_2$. The complexes formed have low photodetachment cross sections at photon energies near the adiabatic binding energy, resulting in high vertical detachment energies. They are therefore reactive radicals with several low-lying excited electronic states, and they are strongly bound anions, both in terms of dissociation to the separate molecular constituents and in terms of removing the electron. A more thorough picture of the electronic structure of the $[O_2$–glyoxal$]^-$ complex anion may lead to better understanding of, as one example, its potential role in the atmospheric chemistry of microclimates defined by biomass burning.[145] Partial bond formation between two molecules with positive EAs was shown to be nuanced in that the difference between the EAs is not the sole governing factor. There are numerous additional atmospherically relevant ketones and aldehydes that could likewise form unique, complex anions with the superoxide anion.

Finally, application of this technique to neutral radical reaction complexes has provided valuable insights into the dynamics of these reactions. These experiments can readily be broadened to include participating of water molecules that would complex with the anions in the troposphere, which would influence the dynamics of the radical reaction complexes. Solvation in related, larger molecular cluster anions have already been shown to drive "core switching", in reference to the identity of the distinct (core) charge carrier in the cluster.[39,40,74,146] A change in electron distribution in the complex will certainly affect the reaction dynamics.

Anion photodetachment spectroscopies offer a powerful tool for the study of a diverse array of atmospherically relevant species and could shed further insight into pieces in the complex puzzle the troposphere presents.

## AUTHOR INFORMATION

### Corresponding Author

**Caroline Chick Jarrold** – *Department of Chemistry, Indiana University, Avenue Bloomington, Indiana 47405, United States;* orcid.org/0000-0001-9725-4581; Email: cjarrold@indiana.edu

Complete contact information is available at: https://pubs.acs.org/10.1021/acsphyschemau.2c00060



https://doi.org/10.1021/acsphyschemau.2c00060
ACS Phys. Chem Au 2023, 3, 17–29

## Notes

The author declares no competing financial interest.

## ■ ACKNOWLEDGMENTS

The author gratefully acknowledges support for this research from the National Science Foundation, Grant No. CHE-2053889

## ■ REFERENCES

(1) Felton, J. A.; Ray, M.; Jarrold, C. C. Measurement of the Electron Affinity of Atomic Ce. *Phys. Rev. A* **2014**, *89*, 033047.
(2) Schaefer, B.; Pal, R.; Khetrapal, N. S.; Amsler, M.; Sadeghi, A.; Blum, V.; Zeng, X. C.; Goedecker, S.; Wang, L.-S. Isomerism and Structural Fluxionality in the $Au_{26}$ and $Au_{26}^-$ Nanoclusters. *ACS Nano* **2014**, *8*, 7413−7422.
(3) Hirata, K.; Ito, S.; Kim, K.; Nakamura, K.; Kitazawa, H.; Hayashi, S.; Koyasu, K.; Tsukuda, T. Correction to "Photoinduced Thermionic Emission from $[M_{25}(SR)_{18}]^-$ (M = Au, Ag) Revealed by Anion Photoelectron Spectroscopy. *J. Phys. Chem. C* **2022**, *126*, 8965−8966.
(4) Henley, A.; Fielding, H. H. Anion Photoelectron Spectroscopy of Protein Chromophores. *Int. Rev. Phys. Chem.* **2019**, *38*, 1−34.
(5) Continetti, R. E.; Guo, H. Dynamics of Transient Species via Anion Photodetachment. *Chem. Soc. Rev.* **2017**, *46*, 7650−7667.
(6) Novick, S. E.; Engelking, P. C.; Jones, P. L.; Futrell, J. H.; Lineberger, W. C. Laser Photoelectron, Photodetachment, and Photodestruction Spectra of $O_3^-$. *J. Chem. Phys.* **1979**, *70*, 2652−2662.
(7) Arnold, D. W.; Xu, C.; Kim, E. H.; Neumark, D. M. Study of the Low-Lying Electronic States of Ozone by Anion Photoelectron Spectroscopy. *J. Chem. Phys.* **1994**, *101*, 912−922.
(8) Villano, S. M.; Eyet, N.; Wren, S. W.; Ellison, G. B.; Bierbaum, V. M.; Lineberger, W. C. Photoelectron Spectroscopy and Thermochemistry of the Peroxyformate Anion. *J. Phys. Chem. A* **2010**, *114*, 191−200.
(9) Wang, X.-B.; Nicholas, J. B.; Wang, L.-S. Photoelectron Spectroscopy and Theoretical Calculations of $SO_4^-$ and $HSO_4^-$: Confirmation of High Electron Affinities of $SO_4$ and $HSO_4$. *J. Phys. Chem. A* **2000**, *104*, 504−508.
(10) Patros, K. M.; Mann, J. E.; Dobulis, M. A.; Thompson, M. C.; Jarrold, C. C. Probing Alkenoxy Radical Electronic Structure using Anion PEI Spectroscopy. *J. Chem. Phys.* **2019**, *150*, 034302.
(11) Ramond, T. M.; Blanksby, S. J.; Kato, S.; Bierbaum, V. M.; Davico, G. E.; Schwartz, R. L.; Lineberger, C. W.; Ellison, G. B. Heat of Formation of the Hydroperoxyl Radical HOO Via Negative Ion Studies. *J. Phys. Chem. A* **2002**, *106*, 9641−9647.
(12) Oliveira, A. M.; Lehman, J. H.; McCoy, A. B.; Lineberger, W. C. Photoelectron Spectroscopy of *cis*-Nitrous Acid Anion (*cis*-$HONO^-$). *J. Phys. Chem. A* **2016**, *120*, 1652−1660.
(13) Oliveira, A. M.; Lehman, J. H.; McCoy, A. B.; Lineberger, W. C. Photoelectron Spectroscopy of the Hydroxymethoxide Anion, $H_2C(OH)O^-$. *J. Chem. Phys.* **2016**, *145*, 124317.
(14) Weaver, A.; Arnold, D. W.; Bradforth, S. E.; Neumark, D. M. Examination of the $^3A_2'$ and $^2E''$ States of $NO_3$ by Ultraviolet Photoelectron Spectroscopy of $NO_3^-$. *J. Chem. Phys.* **1991**, *94*, 1740−1751.
(15) DeWitt, M.; Babin, M. C.; Neumark, D. M. High-Resolution Photoelectron Spectroscopy of Vibrationally Excited $OH^-$. *J. Phys. Chem. A* **2021**, *125*, 7260−7265.
(16) Dobulis, M. A.; Thompson, M. C.; Jarrold, C. C. Identification of Isoprene Oxidation Reaction Products via Anion Photoelectron Spectroscopy. *J. Phys. Chem. A* **2021**, *125*, 10089−10102.
(17) Nimlos, M. R.; Ellison, G. B. Photoelectron Spectroscopy of Sulfur-Containing Anions ($SO_2^-$, $S_3^-$ and $S_2O^-$). *J. Phys. Chem.* **1986**, *90*, 2574−2580.
(18) Ervin, K. M.; Ho, J.; Lineberger, W. C. Ultraviolet Photoelectron Spectrum of $NO_2^-$. *J. Phys. Chem.* **1988**, *92*, 5405−5412.
(19) Markus, C. R.; Asvany, O.; Salomon, T.; Schmid, P. C.; Brünken, S.; Lipparini, F.; Gauss, J.; Schlemmer, S. Vibrational Excitation Hindering an Ion−Molecule Reaction: The $c$-$C_3H_2^+$−$H_2$ Collision Complex. *Phys. Rev. Lett.* **2020**, *124*, 223401.
(20) Squires, R. R.; Bierbaum, V. M.; Grabowski, J. J.; DePuy, C. H. Multiple Proton Transfers within Long-Lived Ion Molecule Complexes. *J. Am. Chem. Soc.* **1983**, *105*, 5185−5192.
(21) Ingemann, S.; Nibbering, N. M. M.; Sullivan, S. A.; DePuy, C. H. Nucleophilic Aromatic Substitution in the Gas Phase: The Importance of Fluoride Ion−Molecule Complexes Formed in Gas-Phase Reactions Between Nucleophiles and Some Alkyl Pentafluorophenyl Ethers. *J. Am. Chem. Soc.* **1982**, *104*, 6520−6527.
(22) Willey, K. F.; Cheng, P. Y.; Bishop, M. B.; Duncan, M. A. Charge-Transfer Photochemistry in Ion−Molecule Complexes of Silver. *J. Am. Chem. Soc.* **1991**, *113*, 4721−4728.
(23) Yang, X.; Hu, Y.; Yang, S. Photoinduced Reactions in the Ion−Molecule Complexes $Mg^+$-$XCH_3$ (X = F, Cl). *J. Phys. Chem. A* **2000**, *104*, 8496−8504.
(24) Morton, T. H. Ion Molecule Complexes in Unimolecular Fragmentation of Gaseous Cations. Alkyl Phenyl Ether Molecular Ions. *J. Am. Chem. Soc.* **1980**, *102*, 1596−1602.
(25) Sheng, H.; Tang, W.; Yerabolu, R.; Max, J.; Kotha, R. R.; Riedeman, J. S.; Nash, J. J.; Zhang, M.; Kenttämaa, H. I. Identification of *N*-Oxide and Sulfoxide Functionalities in Protonated Drug Metabolites by Using Ion-Molecular Reactions Followed by Collisionally Activated Dissociation in a Linear Quadrupole Ion Trap Mass Spectrometer. *J. Org. Chem.* **2016**, *81*, 575−586.
(26) Zhu, H.; Ma, X.; Kong, J. Y.; Zhang, M.; Kenttämaa, H. I. Identification of Carboxylate, Phosphate, and Phenoxide Functionalities in Deprotonated Molecules Related to Drug Metabolites via Ion−Molecule Reactions with Water and Diethylhydroxyborane. *J. Am. Mass Spectrom.* **2017**, *28*, 2189−2200.
(27) Wu, C.-X.; Hu, J.; He, M.-M.; Zhi, Y.; Tian, S. X. Ion Momentum Imaging Study of the Ion−Molecule Reaction $Ar^+ + O_2 \rightarrow O_2^+ + Ar$. *Phys. Chem. Chem. Phys.* **2020**, *22*, 4640−4646.
(28) Thøgersen, J.; Réhault, J.; Odelius, M.; Ogden, T.; Jena, N. K.; Jensen, S. J. K.; Keiding, S. R.; Helbing, J. Hydration Dynamics of Aqueous Nitrate. *J. Phys. Chem. B* **2013**, *117*, 3376−3388.
(29) Yuan, R.; Yan, C.; Fayer, M. Ion−Molecule Complex Dissociation and Formation Dynamics in LiCl Aqueous Solutions from 2D IR Spectroscopy. *J. Phys. Chem. B* **2018**, *122*, 10582−10592.
(30) Waterland, M. R.; Stockwell, D.; Kelley, A. M. Symmetry Breaking Effects of $NO_3^-$: Raman Spectra of Nitrate Salts and *Ab Initio* Resonance Raman Spectra of Nitrate-Water Complexes. *J. Chem. Phys.* **2001**, *114*, 6249−6258.
(31) Vuitton, V.; Yelle, R. V.; Klippenstein, S. J.; Hörst, S. M.; Lavvas, P. Simulating the Density of Organic Species in the Atmosphere of Titan With a Coupled Ion-Neutral Photochemical Model. *Icarus* **2019**, *324*, 120−197.
(32) Larsson, M.; Geppert, W. D.; Nyman, G. Ion Chemistry in Space. *Rep. Prog. Phys.* **2012**, *75*, 066901.
(33) Viggiano, A. A. Reexamination of Ionospheric Chemistry: High Temperature Kinetics, Internal Energy Dependences, Usual Isomers, and Corrections. *Phys. Chem. Chem. Phys.* **2006**, *8*, 2557−2571.
(34) Anicich, V. G.; McEwan, M. J. Ion−Molecule Chemistry in Titan's Ionosphere. *Plan. Space Sci.* **1997**, *45*, 897−921.
(35) Richards, D. S.; Trobaugh, K. L.; Hajek-Herrera, J.; Price, C. L.; Sheldon, C. S.; Davies, J. F.; Davis, R. D. Ion−Molecule Interactions Enable Unexpected Phase Transitions in Organic-Inorganic Aerosol. *Sci. Adv.* **2020**, *6*, No. eabb5643.
(36) Lu, Y.-J.; Lehman, J. H.; Lineberger, W. C. A Versatile, Pulsed Anion Source Utilizing Plasma-Entrainment: Characterization and Applications. *J. Chem. Phys.* **2015**, *142*, 044201.
(37) Dobulis, M. A.; Thompson, M. C.; Sommerfeld, T.; Jarrold, C. C. Temporary Anion States of Fluorine Substituted Benzenes Probed by Charge Transfer in $O_2^-$•$C_6H_{6-x}F_x$ ($x$ = 0−5) Ion−Molecule Complexes. *J. Chem. Phys.* **2020**, *152*, 204309.
(38) Schwartz, R.; Davico, G. E.; Kim, J. B.; Lineberger, W. C. Negative Ion Photoelectron Spectroscopy of $OH^-(NH_3)$. *J. Chem. Phys.* **2000**, *112*, 4966−4973.
(39) Khuseynov, D.; Goebbert, D. J.; Sanov, A. Oxygen Cluster Anions Revisted: Solvent-Mediated Dissociation of the Core $O_4^-$ Anion. *J. Chem. Phys.* **2012**, *136*, 094312.

(40) Pichugin, K.; Grumbling, E.; Velarde, L.; Sanov, A. Solvation-Induced Cluster Anion Core Switching from $NNO_2^-(N_2O)_{n-1}$ to $O^-(N_2O)_n$. *J. Chem. Phys.* **2008**, *129*, 044311.
(41) Lietard, A.; Mensa-Bonsu, G.; Verlet, J. R. R. The Effect of Solvation on Electron Capture Revealed Using Anion Two-Dimensional Photoelectron Spectroscopy. *Nat. Chem.* **2021**, *13*, 737−742.
(42) Sanov, A. Intermolecular Interactions in Cluster Anions. *Int. Rev. Phys. Chem.* **2021**, *40*, 495−545.
(43) Mbaiwa, F.; Wei, J.; Van Duzor, M.; Mabbs, R. Threshold Effects in $I^-\cdot CH_3CN$ and $I^-\cdot H_2O$ Cluster Anion Detachment: The Angular Distribution as an Indicator of Electronic Autodetachment. *J. Chem. Phys.* **2010**, *132*, 134304.
(44) Mbaiwa, F.; Holtgrewe, N.; Dao, D. B.; Lasinski, J.; Mabbs, R. Photoelectron Angular Distributions as Probes of Cluster Anion Structure: $I^-\cdot(H_2O)_2$ and $I^-\cdot(CH_3CN)_2$. *J. Phys. Chem. A* **2014**, *118*, 7249−7254.
(45) Le Barbu, K.; Schiedt, J.; Weinkauf, R.; Schlag, E. W.; Nilles, J. M.; Xu, S.-J.; Thomas, O. C.; Bowen, K. H. Microsolvation of Small Anions by Aromatic Molecules: An Exploratory Study. *J. Chem. Phys.* **2002**, *116*, 9663−9671.
(46) Hendricks, J. H.; de Clercq, H. L.; Freidhoff, C. B.; Arnold, S. T.; Eaton, J. G.; Fancher, C.; Lyapustina, S. A.; Snodgrass, J. T.; Bowen, K. H. Anion solvation at the Microscopic Level: Photoelectron Spectroscopy and the Solvated Anion Clusters, $NO^-(Y)_n$, where Y = Ar, Kr, Xe, $N_2O$, $H_2S$, $NH_3$, $H_2O$ and $C_2H_4(OH)_2$. *J. Chem. Phys.* **2002**, *116*, 7926−7938.
(47) Arnold, S. T.; Hendricks, J. H.; Bowen, K. H. Photoelectron Spectroscopy of the Solvated Anions Clusters $O^-(Ar)_n$ (n = 1−26, 34: Energetics and Structure. *J. Chem. Phys.* **1995**, *102*, 39−47.
(48) Wang, X.-B. Cluster Model Studies of Anion and Molecular Specificities via Electrospray ionization Photoelectron Spectroscopy. *J. Phys. Chem. A* **2017**, *121*, 1389−1401.
(49) Wang, X.-B.; Sergeeva, A. P.; Yang, J.; Xing, X.-P.; Boldyrev, A. I.; Wang, L.-S. Photoelectron Spectroscopy of Cold Hydrated Sulfate Cluters, $SO_4^{2-}(H_2O)_n$ (n = 4−7); Temperature-Dependent Isomer Populations. *J. Phys. Chem. A* **2009**, *113*, 5567−5576.
(50) Koga, M.; Asplund, M.; Neumark, D. M. Electron Attachment Dynamics Following UV Excitation of Iodide-2-Thiouracil Complexes. *J. Chem. Phys.* **2022**, *156*, 244302.
(51) Li, W. L.; Kunin, A.; Matthews, E.; Yoshikawa, N.; Dessent, C. E. H.; Neumark, D. M. Photodissociation Dynamics of the Iodide-Uracil (I-U) Complex. *J. Chem. Phys.* **2016**, *145*, 044319.
(52) Zhao, Y. X.; Yourshaw, I.; Reiser, G.; Arnold, C. C.; Neumark, D. M. Study of the $ArBr^-$, $ArI^-$, and $KrI^-$ Anions and the Corresponding Neutral van der Waals Complexes by Anion Zero Electron Kinetic Energy Spectroscopy. *J. Chem. Phys.* **1994**, *101*, 6538−6551.
(53) Yan, C.; Dada, L.; Rose, C.; Jokinen, T.; Nie, W.; Schobesberger, S.; Junninen, H.; Lehtipalo, K.; Sarnela, N.; Makkonen, U.; Garmash, O.; Wang, Y.; Zha, Q.; Paasonen, P.; Bianchi, F.; Sipila, M.; Ehn, M.; Petaja, T.; Kerminen, V.-M.; Worsnop, D. R.; Kulmala, M. The Role of $H_2SO_4$-$NH_3$ Anion Clusters in Ion-Induced Aerosol Nucleation Mechanisms in the Boreal Forest. *Atmos. Chem. Phys.* **2018**, *18*, 13231−13243.
(54) Shuman, N. S.; Hunton, D. E.; Viggiano, A. A. Ambient and Modified Atmospheric Ion Chemistry: From Top to Bottom. *Chem. Rev.* **2015**, *115*, 4542−4570.
(55) Li, M.; Karu, E.; Brenninkmeijer, C.; Fischer, H.; Lelieveld, J.; Williams, J. Tropospheric OH and Stratospheric OH and Cl Concentrations Determined from $CH_4$, $CH_3Cl$, and $SF_6$ Measurements. *npj Clim. Atmos. Sci.* **2018**, *1*, 29.
(56) Laakso, L.; Petaja, T.; Lehtinen, K. E. J.; Kulmala, M.; Paatero, J.; Horrak, U.; Tammet, H.; Joutsensaari, J. Ion Production Rate in a Boreal Forest based on Ion, Particle and Radiation Measurements. *Atmos. Chem. Phys.* **2004**, *4*, 1933−1943.
(57) Luts, A.; Parts, T.-E.; Laakso, L.; Hirsikko, A.; Gronholm, T.; Kulmala, M. Some Air Electricity Phenomena Caused by Waterfalls: Correlative Study of the Spectra. *Atmos. Res.* **2009**, *91*, 229−237.
(58) Kohler, S. J.; Lofgren, S.; Wilander, A.; Bishop, K. Validating a Simple Equation to Predict and Analyze Organic Anion Charge in Swedish Low Ionic Strength Surface Waters. *Water Air Soil Pollut.* **2001**, *130*, 799−804.
(59) Luts, A.; Parts, T. Evolution of Negative Small Air Ions at Two Different Temperatures. *J. Atmos. Solar-Terr. Phys.* **2002**, *64*, 763−774.
(60) Posey, L. A.; Deluca, M. J.; Johnson, M. A. Demonstration of a Pulsed Photoelectron Spectrometer on Mass-Selected Negative Ions: $O^-$, $O_2^-$ and $O_4^-$. *Chem. Phys. Lett.* **1986**, *131*, 170−174.
(61) Sherwood, C. R.; Garner, M. C.; Hanold, K. A.; Strong, K. M.; Continetti, R. E. Energy and Angular Distributions in Dissociative Photodetachment of $O_4^-$. *J. Chem. Phys.* **1995**, *102*, 6949−6952.
(62) Sherwood, C. R.; Hanold, K. A.; Garner, M. C.; Strong, K. M.; Continetti, R. E. Translational Spectroscopy Studies of the Photodissociation Dynamics of $O_4^-$. *J. Chem. Phys.* **1996**, *105*, 10803−10811.
(63) Hanold, K. A.; Continetti, R. E. Photoelectron-Photofragment Coincidence studies of the Dissociative Photodetachment of $O_4^-$. *Chem. Phys.* **1998**, *239*, 493−509.
(64) Arnold, D. W.; Neumark, D. M. Study of $N_2O_2$ by Photoelectron Spectroscopy of $N_2O_2^-$. *J. Chem. Phys.* **1995**, *102*, 7035−7045.
(65) Dauletyarov, Y.; Wallace, A. A.; Blackstone, C. C.; Sanov, A. Photoelectron Spectroscopy of Biacetyl and Its Cluster Anions. *J. Phys. Chem. A* **2019**, *123*, 4158−4167.
(66) Mensa-Bonsu, G.; Wilson, M. R.; Tozer, D. J.; Verlet, J. R. R. Photoelectron Spectroscopy of *para*-Benzoquinone Cluster Anions. *J. Chem. Phys.* **2019**, *151*, 204302.
(67) Liu, G.; Diaz-Tinoco, M.; Ciborowski, S. M.; Martinez-Martinez, C.; Lyapustina, S.; Hendricks, J. H.; Ortiz, J. V.; Bowen, K. H. Excess Electrons Bound to $H_2S$ Trimer and Tetramer Clusters. *Phys. Chem. Chem. Phys.* **2020**, *22*, 3273−3280.
(68) Coe, J. V.; Williams, S. M.; Bowen, K. H. Photoelectron Spectra of Hydrated Electron Clusters vs. Cluster Size: Connecting to Bulk. *Int. Rev. Phys. Chem.* **2008**, *27*, 27−51.
(69) Young, R. M.; Yandell, M. A.; Niemeyer, M.; Neumark, D. M. Photoelectron Imaging of Tetrahydrofuran Cluster Anions $(THF)_n^-$ ($1 \leq n \leq 100$). *J. Chem. Phys.* **2010**, *133*, 154312.
(70) Mann, J. E.; Troyer, M. E.; Jarrold, C. C. Photoelectron Imaging and Photodissociation of Ozonide in $O_3^-\bullet(O_2)_n$ ($n = 1-4$) Clusters. *J. Chem. Phys.* **2015**, *142*, 124305.
(71) Ervin, K. M.; Anusiewicz, I.; Skurski, P.; Simons, J.; Lineberger, W. C. The Only Stable State of $O_2^-$ is the X $^2\Pi_g$ Ground State and It (Still!) Has an Adiabatic Electron Detachment Energy of 0.45 eV. *J. Phys. Chem. A* **2003**, *107*, 8521−8529.
(72) Buntine, M. A.; Lavrich, D. J.; Dessent, C. E.; Scarton, M.G.; Johnson, M. A. Photoinitiation of the $O^- + H_2O \cdot OH^- + OH$ Ion−Molecule Reaction within the $O_2^-\cdot H_2O$ Binary Complex. *Chem. Phys. Lett.* **1993**, *216*, 471−478.
(73) Sherwood, C. R.; Continetti, R. E. Dissociative Photodetachment Dynamics of $O_2^-\cdot(H_2O)$. *Chem. Phys. Lett.* **1996**, *258*, 171−179.
(74) Goebbert, D. J.; Sanov, A. Photodetachment, Photofragmentation, and Fragment Autodetachment of $[O_{2n}(H_2O)_m]^-$ clusters; Core-anion Structures and Fragment Energy Partitioning. *J. Chem. Phys.* **2009**, *131*, 104308.
(75) Akin, F. A.; Schirra, L. K.; Sanov, A. Photoelectron Imaging Study of the Effect of Monohydration on $O_2^-$ Photodetachment. *J. Phys. Chem. A* **2006**, *110*, 8031−8036.
(76) Luong, A. K.; Clements, T. G.; Sowa Resat, M.; Continetti, R. E. Energetics and Dissociative Photodetachment Dynamics of Superoxide-Water Clusters: $O_2^-(H_2O)_n$, n = 1−6. *J. Chem. Phys.* **2001**, *114*, 3449−3455.
(77) Crawford, M. F.; Welsh, H. L.; Locke, J. L. Infra-Red Absorption of Oxygen and Nitrogen Induced by Intermolecular Forces. *Phys. Rev.* **1949**, *75*, 1607−1607.
(78) Finlayson-Pitts, B. J.; Pitts, J. N., Jr.*Chemistry of the Upper and Lower Atmosphere: Theory, Experiments and Applications*; Academic Press: San Diego, CA, 2000; p 89, DOI: 10.1016/B978-0-12-257060-5.X5000-X.
(79) Richard, C.; Gordon, I. E.; Rothman, L. S.; Abel, M.; Frommhold, L.; Gustafsson, M.; Hartmann, J. M.; Hermans, C.; Lafferty, W. J.; Orton, G. S.; Smith, K. M.; Tran, H. New Section of the HITRAN

Database: Collision-Induced Absorption (CIA). *J. Quant. Spectrosc. Radiat. Transfer* **2012**, *113*, 1276−1285.
(80) Zender, C. S. Global Climatology of Abundance and Solar Absorption of Oxygen Collision Complexes. *J. Geophys. Res.* **1999**, *104*, 24471−24484.
(81) Thalman, R.; Volkamer, R. Temperature Dependent Absorption Cross-Sections of $O_2$-$O_2$ Collision Pairs between 340 and 630 nm and at Atmospherically Relevant Pressure. *Phys. Chem. Chem. Phys.* **2013**, *15*, 15371−15381.
(82) Karman, T.; Gordon, I. E.; van der Avoird, A.; Baranov, Y. I.; Boulet, C.; Drouin, B. J.; Groenenboom, G. C.; Gustafsson, M.; Hartmann, J.-M.; Kurucz, R. L.; Rothman, L. S.; Sun, K.; Sung, K.; Thalman, R.; Tran, H.; Wishnow, E. H.; Wordsworth, R.; Vigasin, A. A.; Volkamer, R.; van der Zande, W. J. Update of the HITRAN Collision-Induced Absorption Section. *Icarus* **2019**, *328*, 160−175.
(83) Patros, K. M.; Mann, J. E.; Jarrold, C. C. Photoelectron Imaging Spectra of $O_2^-$•VOC and $O_4^-$•VOC Complexes. *J. Phys. Chem. A* **2016**, *120*, 7828−7838.
(84) Patros, K. M.; Mann, J. E.; Jarrold, C. C. $O_2^-$•[Polar VOC] Complexes: H-Bonding versus Charge-Dipole Interactions, and the Noninnocence of Formaldehyde. *J. Phys. Chem. A* **2017**, *121*, 5459−5467.
(85) Naus, H.; Ubachs, W. Visible absorption bands of the $(O_2)_2$ Collision Complex at Pressures Below 760 Torr. *Appl. Opt.* **1999**, *38*, 3423−3428.
(86) Parsons, B. F.; Freitag, M. A.; Warder, H. J. Singlet $O_2$ Produced by Ultraviolet Dissociation of the $\beta$-ionone−$O_2$ Complex. *J. Phys. Chem. A* **2021**, *125*, 8649−8657.
(87) Baklanov, A. V.; Parker, D. H. Weakly Bound Environment of Molecular Oxygen as a Catalyst of Photooxidation. *Kinet. Catal.* **2020**, *61*, 174−197.
(88) Parsons, B. F.; Chandler, D. W. On the Dissociation of van der Waals Clusters of $X_2$−Cyclohexane (X = O, Cl) Following Charge-Transfer Excitation in the Ultraviolet. *J. Phys. Chem. A* **2003**, *107*, 10544−10553.
(89) Bogomolov, A. S.; Dozmorov, N. V.; Kochubei, S. A.; Baklanov, A. V. REMPI Detection of Singlet Oxygen $^1O_2$ arising from UV-Photodissociation of van der Waals Complex Isoprene-Oxygen $C_5H_8$-$O_2$. *Chem. Phys. Lett.* **2018**, *692*, 271−276.
(90) Vidma, K. V.; Frederix, P. W. J. M.; Parker, D. H.; Baklanov, A. V. Photodissociation of van der Waals Clusters of Isoprene With Oxygen, $C_5H_8$−$O_2$, in the Wavelength Range 213−277 nm. *J. Chem. Phys.* **2012**, *137*, 054305.
(91) Baklanov, A. V.; Bogdanchikov, G. A.; Vidma, K. V.; Chestakov, D. A.; Parker, D. H. Cluster-Enhanced X-$O_2$ Photochemistry (X = $CH_3O$, $C_3H_6$, $C_6H_{12}$, and Xe). *J. Chem. Phys.* **2007**, *126*, 124316.
(92) Baklanov, A. V.; Bogomolov, A. S.; Pyryaeva, A. P.; Bogdanchikov, G. A.; Kochubei, S. A.; Farooq, Z.; Parker, D. H. Singlet Oxygen Photogeneration from X−$O_2$ van der Waals Complexes: Double Spin-flip vs. Charge-transfer Mechanism. *Phys. Chem. Chem. Phys.* **2015**, *17*, 28565−28573.
(93) Pyryaeva, A. P.; Ershov, K. S.; Kochubei, S. A.; Baklanov, A. V. Singlet Oxygen Generation via UV-A. -B, and -C Photoexcitation of Isoprene-Oxygen ($C_5H_8$-$O_2$) Encounter Complexes in the Gas Phase. *J. Phys. Chem. A* **2020**, *124*, 8469−8477.
(94) Dauletyarov, Y.; Sanov, A. Weak Covalent Interactions and Anionic Charge-Sharing Polymerisation in Cluster Environments. *Phys. Chem. Chem. Phys.* **2021**, *23*, 11596−11610.
(95) Gibbard, J. A.; Continetti, R. E. Photoelectron Photofragment Coincidence Spectroscopy of Carboxylates. *RSC Adv.* **2021**, *11*, 34250−34261.
(96) Dobulis, M. A.; McGee, C. J.; Sommerfeld, T.; Jarrold, C. C. Autodetachment over Broad Photon Energy Ranges in the Anion Photoelectron Spectra of [O2−M]− (M = Glyoxal, Methylglyoxal, or Biacetyl) Complex Anions. *J. Phys. Chem. A* **2021**, *125*, 9128−9142.
(97) Xue, T.; Dixon, A. R.; Sanov, A. Anion Photoelectron Imaging Spectroscopy of Glyoxal. *Chem. Phys. Lett.* **2016**, *660*, 205−208.
(98) Dauletyarov, Y.; Dixon, A. R.; Wallace, A. A.; Sanov, A. Electron Affinity and Excited States of Methylglyoxal. *J. Chem. Phys.* **2017**, *147*, 013934.
(99) Wittrock, F.; Richter, A.; Oetjen, H.; Burrows, J. P.; Kanakidou, M.; Myriokefalitakis, S.; Volkamer, R.; Beirle, S.; Platt, U.; Wagner, T. Simultaneous Global Observations of Glyoxal and Formaldehyde from Space. *Geophys. Res. Lett.* **2006**, *33*, L16804.
(100) Volkamer, R.; Platt, U.; Wirtz, K. Primary and Secondary Glyoxal Formation from Aromatics: Experimental Evidence for the Bicylcoalkyl-Radical Pathway from Benzene, Toluene, and *p*-Xylene. *J. Phys. Chem. A* **2001**, *105*, 7865−7874.
(101) Carlton, A. G.; Turpin, B. J.; Altieri, K. E.; Seitzinger, S.; Reff, A.; Lim, H.-J.; Ervens, B. Atmospheric Oxalic Acid and SOA Production from Glyoxal: Results of Aqueous Photooxidation Experiments. *Atmos. Environ.* **2007**, *41*, 7588−7602.
(102) Waxman, E. M.; Dzepina, K.; Ervens, B.; Lee-Taylor, J.; Aumont, B.; Jimenez, J. L.; Madronich, S.; Volkamer, R. Secondary Organic Aerosol Formation from Semi- and Intermediate-Volatility Organic Compounds and Glyoxal: Relevance of O/C as a Tracer for Aqueous Multiphase Chemistry. *Geophys. Res. Lett.* **2013**, *40*, 978−982.
(103) Lombardi, M.; Jost, R.; Michel, C.; Tramer, A. Study of Singlet-Triplet Coupling in Glyoxal by Level Anticrossing Spectroscopy. II. Theory of the Positions of Double Resonances Near a Singlet-Triplet Anticrossing. Application to the Precise Measurement of Singlet-Triplet Coupling and of Fine and Hyperfine Structure Parameters of the Triplet of Glyoxal. *Chem. Phys.* **1981**, *57*, 341−353.
(104) Dupre, P.; Jost, R.; Lombardi, M. Study of Singlet-Triplet Coupling in Glyoxal by Level Anticrossing Spectroscopy. V. Nature of the Singlet-Triplet Interaction. *Chem. Phys.* **1984**, *91*, 355−372.
(105) Michel, C.; Tramer, A. Selected Rotational Level Lifetimes and Singlet-Triplet Coupling in the $S_1$ State of Glyoxal. *Chem. Phys.* **1979**, *42*, 315−323.
(106) Anderson, L. G.; Parmenter, C. S.; Poland, H. M. Collision Induced Intersystem Crossing. The Photophysics of Glyoxal Vapor Excited at 4358 Å. *Chem. Phys.* **1973**, *1*, 401−417.
(107) Loge, G. W.; Parmenter, C. S. Collision-Free Dissociation after Excitation of Single Rotational Levels in $S_1$ Glyoxal. *J. Phys. Chem.* **1981**, *85*, 1653−1662.
(108) Yardley, J. T. Collisional Quenching and Photochemistry of *trans*-Glyoxal ($^3A_u$) Molecules. *J. Chem. Phys.* **1972**, *56*, 6192−6197.
(109) Diem, M.; MacDonald, B. G.; Lee, E. K. C. Photolysis and Laser-Excited Fluorescence and Phosphorescence Emission of *trans*-Glyoxal in an Argon Matrix at 13 K. *J. Phys. Chem.* **1981**, *85*, 2227−2232.
(110) Butz, K. W.; Krajnovich, D. J.; Parmenter, C. S. An Experimental Potential Energy Surface for Internal Rotation in Glyoxal. *J. Chem. Phys.* **1990**, *93*, 1557−1567.
(111) Butz, K. W.; Johnson, J. R.; Krajnovich, D. J.; Parmenter, C. S. *Cis*-Glyoxal in Effusive and Supersonic Beams. Spectroscopy, Selective Pumping, and *Cis-Trans* Interconversion. *J. Chem. Phys.* **1987**, *86*, 5923−5939.
(112) Smith, D. F.; McIver, C. D.; Kleindienst, T. E. Primary Product Distribution from the Reaction of Hydroxyl Radicals with Toluene at ppb $NO_x$ Mixing Ratios. *J. Atmos. Chem.* **1998**, *30*, 209−228.
(113) Bandow, H.; Washida, N. Ring-Cleavage Reactions of Aromatic Hydrocarbons Studied by FT-IR Spectroscopy. III. Photooxidation of 1,2,3-, 1,2,4-, and 1,3,5-Trimethylbenzenes in the $NO_x$-Air System. *Bull. Chem. Soc. Jpn.* **1985**, *58*, 2549−2555.
(114) Niki, H.; Maker, P. D.; Savage, C. M.; Breitenbach, L. P.; Hurley, M. D. FTIR Spectroscopic Study of the Mechanism for the Gas-Phase Reaction Between Ozone and Tetramethylethylene. *J. Phys. Chem.* **1987**, *91*, 941−946.
(115) Paulson, S. E.; Seinfeld, J. H. Development and Evaluation of a Photooxidation Mechanism for Isoprene. *J. Geophys. Res. Atmos.* **1992**, *97*, 20703−20715.
(116) De Haan, D. O.; Corrigan, A. L.; Tolbert, M. A.; Jimenez, J. L.; Wood, S. E.; Turley, J. J. Secondary Organic Aerosol Formation by Self-Reaction of Methylglyoxal and Glyoxal in Evaporating Droplets. *Environ. Sci. Technol.* **2009**, *43*, 8184−8190.


https://doi.org/10.1021/acsphyschemau.2c00060
*ACS Phys. Chem Au* 2023, 3, 17−29

(117) Schwier, A. N.; Sareen, N.; Mitroo, D.; Shapiro, E. L.; McNeill, V. F. Glyoxal-Methylglyoxal Cross-Reactions in Secondary Organic Aerosol Formation. *Environ. Sci. Technol.* **2010**, *44*, 6174−6182.
(118) Atkinson, R.; Aschmann, S. M. Products of the Gas-Phase Reactions of Aromatic Hydrocarbons: Effects of $NO_2$ Concentration. *Int. J. Chem. Kinet.* **1994**, *26*, 929−944.
(119) Atkinson, R. Atmospheric Chemistry of VOCs and $NO_x$. *Atmos. Environ.* **2000**, *34*, 2063−2101.
(120) Faust, B. C.; Powell, K.; Rao, C. J.; Anastasio, C. Aqueous-Phase Photolysis of Biacetyl (an $\alpha$-Dicarbonyl Compound): A Sink for Biacetyl, and a Source of Acetic Acid, Peroxyacetic Acid, Hydrogen Peroxide, and the Highly Oxidizing Acetylperoxyl Radical in Aqueous Aerosols, Fogs, and Clouds. *Atmos. Environ.* **1997**, *31*, 497−510.
(121) Chen, Y.; Wang, W.; Zhu, L. Wavelength-Dependent Photolysis of Methylglyoxal in the 290−440 nm Region. *J. Phys. Chem. A* **2000**, *104*, 11126−11131.
(122) Kaya, K.; Harshbarger, W. R.; Robin, M. B. Triplet States of Biacetyl and Energy Transfer as Revealed by Opto-Acoustic Spectroscopy. *J. Chem. Phys.* **1974**, *60*, 4231−4236.
(123) Chaiken, J.; Gurnick, M.; McDonald, J. D. Average Singlet-Triplet Coupling Properties of Biacetyl and Methylglyoxal Using Quantum Beat Spectroscopy. *J. Chem. Phys.* **1981**, *74*, 106−116.
(124) Verhaart, G. J.; Brongersma, H. H. Triplet $\pi\rightarrow\pi^*$ and $\pi\rightarrow\pi^*$ Transitions in Glyoxal and Biacetyl by Low-Energy Electron-Impact Spectroscopy. *Chem. Phys. Lett.* **1980**, *72*, 176−180.
(125) Senent, M.L.; Moule, D.C.; Smeyers, Y.G.; Torolabbe, A.; Peqalver, F.J. A Theoretical Spectroscopic Study of the $\tilde{A}\ ^1A_u\ (S_1) \leftarrow \tilde{X}^1A_g(S_0)$, $n\rightarrow\pi^*$ Transition in Biacetyl, $(CH_3CO)_2$. *J. Mol. Spectrosc.* **1994**, *164*, 66−78.
(126) Horowitz, A.; Meller, R.; Moortgat, G. K. The UV-Vis Absorption Cross Sections of $\alpha$-Dicarbonyl Compounds: Pyruvic Acid, Biacetyl, and Glyoxal. *J. Photochem. Photobiol., A* **2001**, *146*, 19−27.
(127) Senent, M.L.; Moule, D.C.; Smeyers, Y.G.; Torolabbe, A.; Peqalver, F.J. A Theoretical Spectroscopic Study of the $\tilde{A}\ ^1A_u\ (S_1) \leftarrow \tilde{X}^1A_g(S_0)$, $n\rightarrow\pi^*$ Transition in Biacetyl, $(CH_3CO)_2$. *J. Mol. Spectrosc.* **1994**, *164*, 66−78.
(128) Opila, R. L.; Coveleskie, R. A.; Yardley, J. T. Spectroscopic Confirmation of Reversible Electronic Energy Transfer in Methylglyoxal. *J. Chem. Phys.* **1975**, *63*, 593−594.
(129) Hammer, N. I.; Diri, K.; Jordan, K. D.; Desfrancois, C.; Compton, R. N. Dipole-Bound Anions of Carbonyl, Nitrile, and Sulfoxide Containing Molecules. *J. Chem. Phys.* **2003**, *119*, 3650−3660.
(130) Jordan, K. D.; Wang, F. Theory of Dipole-Bound Anions. *Annu. Rev. Phys. Chem.* **2003**, *54*, 367−396.
(131) Weber, J. M. The Interaction of Negative Charge with Carbon Dioxide- Insight into Solvation, Speciation, and Reductive Activation from Cluster Studies. *Int. Rev. Phys. Chem.* **2014**, *33*, 489−519.
(132) Schneider, H.; Boese, A. D.; Weber, J. M. Infrared Spectra of $O_2^-\cdot(CO_2)_n$ Clusters ($n$ = 1−6): Asymmetric Docking at the $\pi^*$ Orbital. *J. Chem. Phys.* **2005**, *123*, 074316.
(133) Hiraoka, K.; Yamabe, S. Formation of the Chelate Bonds in the Cluster $O_2^-(CO_2)_n$, $CO_3^-(CO_2)_n$, and $NO_2^-(CO_2)_n$. *J. Chem. Phys.* **1992**, *97*, 643−650.
(134) Lee, S. H.; Kim, N.; Kim, T.-R.; Shin, S.; Kim, S. K. Electron Attachment to the $(O_2\cdots CO_2)$ van der Waals Complex Results in a Monomeric Anion $(O_2\text{-}CO_2)^-$, a Possible Form of $CO_4^-$. *J. Phys. Chem. A* **2021**, *125*, 5794−5799.
(135) Benitez, Y.; Lu, D.; Lunny, K. G.; Li, J.; Guo, H.; Continetti, R. E. Photoelectron-Photofragment Coincidence Studies on Dissociation Dynamics of the OH − $CH_4$ Complex. *J. Phys. Chem. A* **2019**, *123*, 4825−4833.
(136) Benitez, Y.; Parsons, A. J.; Lunny, K. G.; Continetti, R. E. Dissociative Photodetachment Dynamics of the $OH^-(C_2H_4)$ Anion Complex. *J. Phys. Chem. A* **2021**, *125*, 4540−4547.
(137) Benitez, Y.; Nguyen, T. L.; Parsons, A. J.; Stanton, J. F.; Continetti, R. E. Probing the Exit Channel of the OH + $CH_3OH \rightarrow H_2O + CH_3O$ Reaction by Photdetachment of $CH_3O^-(H_2O)$. *J. Phys. Chem. Lett.* **2022**, *13*, 142−148.
(138) Osborn, D. L.; Leahy, D. J.; Kim, E. H.; de Beer, E.; Neumark, D. M. Photoelectron Spectroscopy of $CH_3O^-$ and $CD_3O^-$. *Chem. Phys. Lett.* **1998**, *292*, 651−655.
(139) Nee, M. J.; Osterwalder, A.; Zhou, J.; Neumark, D. M. Slow Electron Velocity-Map Imaging Photoelectron Spectra of the Methoxide Anion. *J. Chem. Phys.* **2006**, *125*, 014306.
(140) Dobulis, M. A.; Thompson, M. C.; Patros, K. M.; Sommerfeld, T.; Jarrold, C. C. Emerging Non-Valence Anion States of [Isoprene-H·]·$H_2O$ Acccessed via Detachment of $OH^-$·Isoprene. *J. Phys. Chem. A* **2020**, *124*, 2279−2287.
(141) Greenwald, E. E.; North, S. W.; Georgievskii, Y.; Klippenstein, S. J. A Two Transition State Model for Radical-Molecule Reactions: Applications to Isomeric Branching in the OH-Isoprene Reaction. *J. Phys. Chem. A* **2007**, *111*, 5582−5592.
(142) Stevens, P. S.; Seymour, E.; Li, Z. Theoretical and Experimental Studies of the Reaction of OH with Isoprene. *J. Phys. Chem. A* **2000**, *104*, 5989−5997.
(143) Peeters, J.; Nguyen, T. L.; Vereecken, L. $HO_x$ Radical Regeneration in the Oxidation of Isoprene. *Phys. Chem. Chem. Phys.* **2009**, *11*, 5935−5939.
(144) Zhang, P.; Chen, T.; Ma, Q.; Chu, B.; Wang, Y.; Mu, Y.; Yu, Y.; He, H. Diesel Soot Photooxidation Enhances the Heterogeneous Formation of $H_2SO_4$. *Nat. Commun.* **2022**, *13*, 5364.
(145) Silva, S. J.; Heald, C. L.; Li, M. Space-Based Constraints on Terrestrial Glyoxal Production. *J. Geog. Res.: Atmos.* **2018**, *123*, 13583−13594.
(146) Mabbs, R.; Surber, E.; Velarde, L.; Sanov, A. Effects of Solvation and Core Switching on the Photoelectron Angular Distributions from $(CO_2)_n^-$ and $(CO)_n^-$·$H_2O$. *J. Chem. Phys.* **2004**, *120*, 5148−5154.


https://doi.org/10.1021/acsphyschemau.2c00060
*ACS Phys. Chem Au* 2023, 3, 17−29